Phase-Based Optical Diffraction Tomography and Intensity Diffraction Tomography

Atsuko Price

Department of Physics and Astronomy, School of Natural Sciences, Rice University

Ideguchi-Group, Department of Physics, University of Tokyo, Tokyo, Japan

Imaging technologies play a crucial role across disciplines including medicine, biology, chemistry, physics, and engineering. As objects of interest shrink to the scale of the imaging wavelength, traditional optical methods face fundamental limitations. Diffraction tomography addresses this challenge by reconstructing the 3D internal structure of a sample based on the perturbations induced in an illuminating light field. This study compares two distinct approaches within diffraction tomography: optical diffraction tomography (ODT), which requires interferometric setups to extract phase and intensity information, and intensity diffraction tomography (IDT), which reconstructs the sample from intensity-only measurements. We derive each method from the inhomogeneous Helmholtz equation, exploring the Born and Rytov approximations used in their respective reconstructions. Using computational simulations, we evaluate ODT and IDT reconstruction quality across varying sample parameters, including refractive index contrast and object radius. Our results demonstrate that ODT is more effective for samples with low refractive index contrast, while IDT outperforms ODT for high-contrast samples. These findings provide a quantitative basis for selecting imaging methods depending on sample characteristics, with implications for future imaging system design and hybrid techniques such as photothermal diffraction tomography.

0 INTRODUCTION

Imaging technology is essential in many fields including, medicine, biology, chemistry, physics, and engineering. More refined imagining technology allows for more accurate or earlier diagnoses of potential issues; whether that be tumors in a human body, micro fractures in a steel beam, or pollutants in water sources. However, imaging the very small can get complicated as the size of the objects being imaged approach in scale to the wavelength of the light imaging it. To combat this, scientists have developed a myriad of ways to image the very small including various methods of microscopy and spectroscopy. In this study, we discuss diffraction tomography, which is used in a type of microscopy. Diffraction tomography reconstructs a 3D image sample based off the way an illuminating coherent light source passing through it, perturbs due to the object. Diffraction is when the bending of light waves around an object occurs. Interference patterns can manifest when multiple diffraction patterns overlap and interact with each other. If they are in-phase they combine to display a region of high intensity, and if they are out-phase they'd combine to create a region of lower intensity. In phase-based optical diffraction tomography (ODT), the phase shift information and intensity information is collected from the scattered field, and an image of the perturbing object is reconstructed from that [1][2]. Due to the use of phase information, the use of a coherent wave front in the illuminating light is essential, thus a interferometric set up is required. In intensity diffraction tomography (IDT), only the intensity information is measured from the scattered field, and the phase information is deduced mathematically from that, so the use of a coherent wave front for the illuminating light here is not necessary [3]. This often means that IDT can be done with less expensive equipment and less accurate of a set up than ODT. [1]

1 THEORY AND METHOD

Diffraction tomography involves the reconstruction of the internal structure of an object by solving and inverse light scattering problem. In this section, the reconstruction algorithms of ODT and IDT and their experimental set ups will be discussed. The theoretical background and methods described in this section are primarily based on the work by P. Muller et al. in "The Theory of Diffraction Tomography" [2].

1.1 ODT Theory

Let's begin with Maxwell's equations for waves.

$$\frac{\partial^2}{\partial t}\Psi(\vec{r},t) = (\frac{c}{n(\vec{r})})^2 \cdot \nabla\Psi(\vec{r},t) \tag{1}$$

However, this includes time independence. This can be simplified to no longer be time dependent.

$$(\nabla^2 + k(r)^2)u(\vec{r}) = 0 \tag{2}$$

$$(\nabla^2 + k_m^2)u_0(\vec{r}) = 0 \tag{3}$$

Which is known as the homogeneous Helmhotlz equation. The solution of this linear partial differential equation has the form,

$$u_o(r) = a_o e^{ik_m\hat{n}\cdot\vec{r}} \tag{4}$$

Now, it is beneficial to use a Green function as a method to solve the inhomogeneous partial differential equation. Green's function is defined as the function G that makes $LG = \delta$ true for a given linear differential operator L and δ being the delta function. In this case, L is $(\nabla^2 + k_m^2)$. So we're trying to find G when

$$(\nabla^2 + k_m^2)G = \delta(r - r') \tag{5}$$

1.1.1 Born Approximation

Next is to linearize the equations, which is to replace nonlinear relationships with simpler approximations to make future calculation easier. This is only valid within a small range, which is fine because small images of weakly scattering objects are being measured. Assume the object only distorts the wave front by small scaling and phase-shifting. When scattering is assumed to be small, the Born Approxmation can be used. The Born Approximation uses the property of the homogeneous component $(\nabla^2 + k_m^2)u_0(\vec{r}) = 0$ to rewrite the inhomogenous equation as

$$(\nabla^2 + k^2)u_o(\vec{r}) = f(\vec{r})u(\vec{r}) \tag{6}$$

Combining this with the delta function which has the translational property

$$\int d^3r'\delta(r - r')g(r') = g(r) \tag{7}$$

yields

$$u_s(\vec{r}) = \int d^3r \cdot G(r - r')f(r')u(r') \tag{8}$$

Since $u = u_o + u_s$

$$u(\vec{r}) = u_o(\vec{r}) + \int d^3r'G(r - r')f(r')u(r') \tag{9}$$

By evaluating equation (8) for u_o and iteratively substituting that into (9), but stopping at the first order Born approximation yields

$$u(\vec{r}) = u_o(\vec{r}) + \int d^3r'G(r - r')f(r')u_o(r') \tag{10}$$

1.1.2 Rytov Approximation

Another approximation method instead of the Born approximation is the Rytov approximation. Born measures direct scattering amplitudes while Rytov measures accumulated phase shifts. While Born linearizes the field, Rytov linearizes the logarithm of the field. Born assumes scattering field is small relative to incident field, which is good for thin samples (relative to wavelength of light), but Rytov assumes that phase distortion is small and smooth but accumulative, which is better for thick samples (relative to the wavelength of light). This means it handles greater phase perturbation better. In the Rytov approximation, linearization by assuming that phase shifting has a natural log relationship is what distinguishes this method from a Born approximation.

$$u(\vec{r}) = u_0(\vec{r}) \cdot e^{\psi(\vec{r})} \tag{11}$$

$$\psi(r) = ln(\frac{u(r)}{u_o(r)}) \tag{12}$$

$$\psi(r) \approx -k^2 \int G(r,r')f(r')d^3r' \tag{13}$$

This integral is a convolution in real space which is hard to compute for. A Fourier Transform would simplify the convolution to a multiplication in Fourier space. A convolution would require time dependece, but with a Fourier Transform you only need to know the frequencies. The Fourier Transform yields this equation in Fourier space

$$u_s\tilde{(}k) = G\tilde{(}k) \cdot \tilde{f}(k) \tag{14}$$

$$f\tilde{(}k) = \frac{u_s\tilde{(}k)}{G\tilde{(}k)} \tag{15}$$

The inverse of this Fourier Transformation

$$f(r) = \mathscr{F}^{-1}[f\tilde{(}k)] \tag{16}$$

yields the refractive index map as a function of real space. This can be used to recover the spatial distribution of refractive index changes to get an image of the perturbing object.

1.2 IDT Theory

Let's revisit the inhomogeneous Helmholtz equation. Assuming weak scattering, apply the Born Approximation and use the Green's function as shown before.

$$u(\vec{r}) = u_o(\vec{r}) + \int d^3r'G(r - r')f(r')u_o(r') \tag{17}$$

The plane wave illumination is given by

$$u_o(\vec{r}|\vec{v_o}) = \sqrt{S(\vec{v_o})}e^{-i(\vec{v_o}\cdot\vec{x}+\eta_o z)} \tag{18}$$

with $\vec{v_o}$ being transverse frequency and η_o being axial frequency. There's an extensive derivation for how to get the scattered field as a 2D Fourier Transform then inversing said Fourier Transform, but the steps are irrelevant for the purposes of this study, so here is the scattered field's final

form.

$$u_s(\vec{x},0|\vec{v}_i) = \frac{ik_o^2}{2}\sqrt{S(\vec{v}_i)}\int \mathscr{F}^{-1}[\Delta\tilde{\varepsilon}(\vec{v}+\vec{v}_i,z')\cdot\frac{e^{-i(\eta(\vec{v})+\eta_i)z'}}{\eta(\vec{v})}]d\vec{v} \tag{19}$$

and the intensity as a function of the scattered field is

$$\tilde{I}(\mathbf{v},0 \mid \mathbf{v}_o) \approx S(\mathbf{v}_o)|P(-\mathbf{v}_o)|^2\delta(\mathbf{v}) + \int [H_{\mathrm{Re}}(\mathbf{v},z \mid \mathbf{v}_o)\Delta\tilde{\varepsilon}_{\mathrm{Re}}(\mathbf{v},z) + H_{\mathrm{Im}}(\mathbf{v},z \mid \mathbf{v}_o)\Delta\tilde{\varepsilon}_{\mathrm{Im}}(\mathbf{v},z)]\, dz \tag{20}$$

where the H_{Re} and H_{Im} are the real and imaginary components of the transfer functions respectively. This intensity function is what is used to reconstruct the image solely from the intensity of the scatter field without the need for phase information.

1.3 Experimental Design

A coherent visible light illuminates a sample stage that has the object, in this case a cell on a slide. The camera reads the reference light or light without the perturbing object and the perturbed light. These are subtracted from each other so that the information left is the perturbed difference. This difference manifests in changes in phase shifts and intensity distribution. The data gathered from this scattered light is used to reconstruct the object/cell in question, along with its internal components using an approximate reconstruction algorithm [1]. In this study computer simulated tests are used to compare these reconstruction algorithms.

$$A(z) = \frac{a_1 + z^{-1}}{1 + a_1 z^{-1}}, \tag{21}$$

2 RESULTS

In this study, we computationally simulated the reconstruction of a computationally generated "ground truth" sphere using both ODT and IDT techniques. The ground truth image used is depicted in Figure 1. Since ODT and IDT are ideal under different parameters, their near-ideal parameters were just found via guess and check.

2.1 ODT Results

The parameters included in tomographic reconstruction include the numerical aperture (NA) of the objective lens, the wavelength of the incident illuminating light, the refractive index of the solution (water), the number of angles at which images were taken, the radius of the "ground truth" sphere, and the refractive index of the "ground truth" sphere. The simulation conditions found near-ideal for ODT are as follows in Table 1:

Table 1. ODT Parameters

Parameter	Value
NA of objective lens	1.1
Wavelength	532 nm
RI of solution	1.33
Number of images	60
Radius of sphere	2 μm
RI of sphere	1.35

The solution is water which has the refractive index of 1.33; this makes the refractive index change by 0.02. In Figures 2-5, the ODT reconstructions from multiple angles are shown. The XY, YZ, and XZ cross-sections are displayed respectively, as well as a XY cross-section that depicts the highest value for that (x,y) at any z called "Maximum Projection."

It can be observed that the reconstruction is not a perfect sphere. There is elongation along the z-axis and artifacts reconstructed all around the main sphere body. These errors are direct results of mathematical approximations (Rytov and Born) and the physical constraints of this experimen-

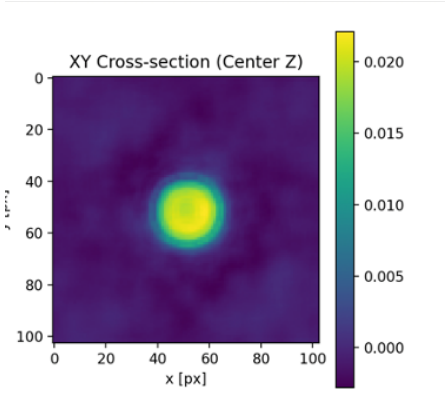

Fig. 2. XY cross-section, centered with z-axis

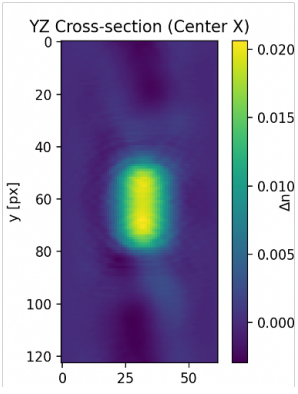

Fig. 3. YZ cross-section, centered with x-axis

Fig. 1. Image of computationally generated "ground truth"

tal set up like limited numerical aperture of the objective lens. The numerical aperture determines which scattered angles you can detect and how much of the 3D Fourier space we can sample. Due to the nature of the limited NA of the lens, an image directly along the Fourier z-axis cannot be taken. This results in a region of missing information around the Fourier z-axis and the elongation of the reconstruction along the z-axis. This same phenomenon occur in the IDT reconstruction as well.

2.2 IDT Results

Using the same "ground truth" image, another image was reconstructed using the IDT reconstruction algorithm. The near-ideal parameters for this reconstruction differs from the ODT near-ideal parameters because IDT reconstruction works better with a smaller NA for the objective lens and a greater RI difference between the solution and the sphere. The new near-ideal parameters reflect this and are displayed in Table 2. Now the RI difference is 0.05 instead of 0.02. In Figures 6-9 the XY, YZ, and XZ cross-sections are shown respectively, as well as a XY cross-section that depicts the highest value for that (x,y) at any z called "Maximum Projection."

It can be observed that the IDT reconstruction seems to show significantly more artifacts than the ODT reconstruction. These artifacts result from the limitations of the approximate mathematical algorithm used in the reconstruction. The reconstruction looks overall less complete than ODT, and the YZ and XZ cross-sections are elongated perpendicularly to the way they were elongated in the ODT reconstruction.

Table 2. IDT Parameters

Parameter	Value
NA of objective lens	0.6
Wavelength	532 nm
RI of solution	1.33
Number of images	60
Radius of sphere	2 μm
RI of sphere	1.38

2.3 Comparisons

Since the NA of the objective lens used for the ODT and IDT reconstruction are vastly different, what would it look like if the same value was used for both. In Figures 10 and 11 the XY Maximum Projection image of ODT and IDT

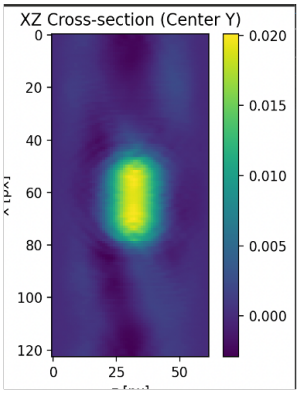

Fig. 4. XZ cross-section, centered with y-axis

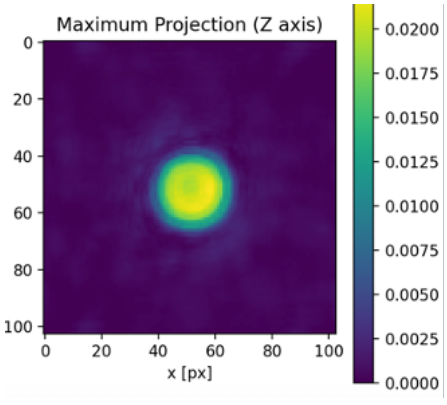

Fig. 5. XY Maximum Projection

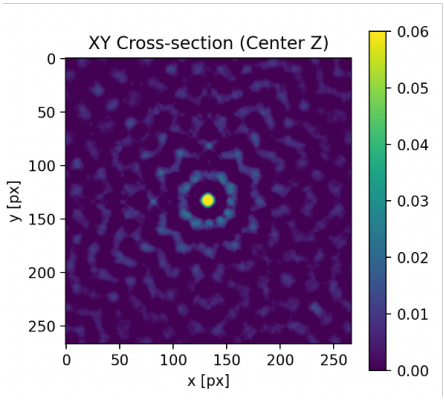

Fig. 6. XY cross-section, centered with z-axis

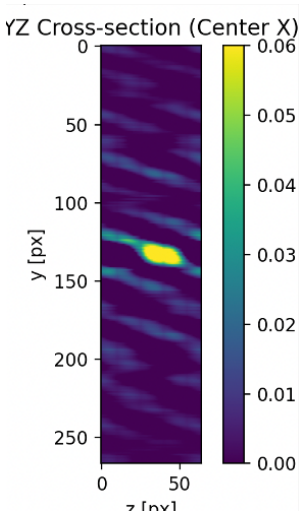

Fig. 7. YZ cross-section, centered with x-axis

reconstructions with the NA at 0.9 and the RI of the sphere at 1.35 can be depicted. The purpose of this is to show the quality of the reconstruction if the same parameters were used, instead of the use of their near-ideal parameters.

The resolution of these reconstructions are worse, as in they display more artifacts, than what they displayed when NA was 1.1 and 0.6 for ODT and IDT respectively. The information surrounding different NA for the objective lens is not crucial because in an experiment, an ideal NA can always be selected for. However, the refractive index of the object being imaged and the size of the object will vary. It is crucial to now how these reconstruction algorithms will behave under varying sphere radii and sphere RI value. Two heatmaps showcasing the relative error between the "ground truth" image and the reconstruction for 20 distinct values of refractive indices and radii were generated. The range of values looked at for radius was from 0.5 μ to 3.0 μ and the range of refractive index differences was from 0.01 to 0.17. These values were selected because they are common cell sizes and cell refractive index differences. For each pair of radius and RI value a reconstruction was made, then squared, then the "ground truth" image was squared, then subtracted from the reconstructed image squared. This left only the artifacts squared which is known in this case as the error. The error was evaluated for ODT and IDT; the resulting heatmaps are shown in Figure 12 and 13.

Both of these heatmaps were generated in their respective near-ideal parameters. So the NA for ODT was at 1.1, and for IDT 0.6, and the RI for ODT was at 1.35, and for IDT 1.38. Purple indicates less error and yellow is more error. It can be observed that for ODT the error increases as RI contrast increases. This behavior is expected, because as the object perturbs the wave front more it should be-

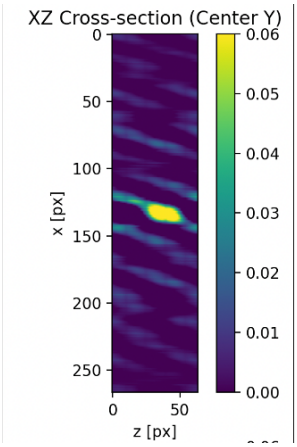

Fig. 8. XZ cross-section, centered with y-axis

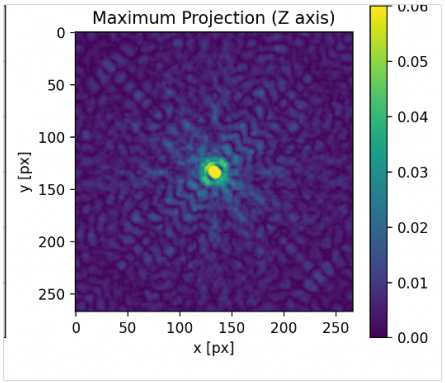

Fig. 9. XY Maximum Projection

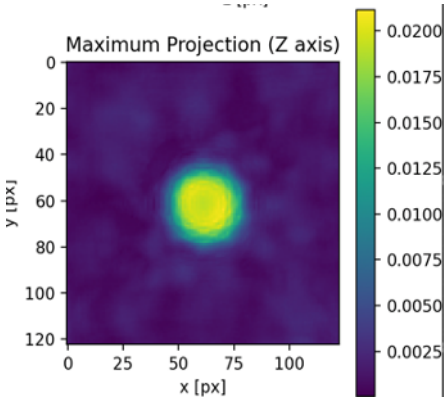

Fig. 10. ODT XY Maximum Projection 0.9 NA

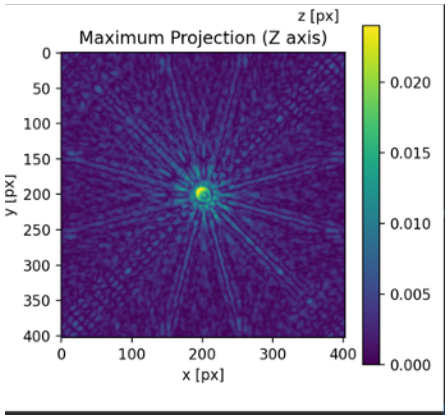

Fig. 11. IDT XY Maximum Projection 0.9 NA

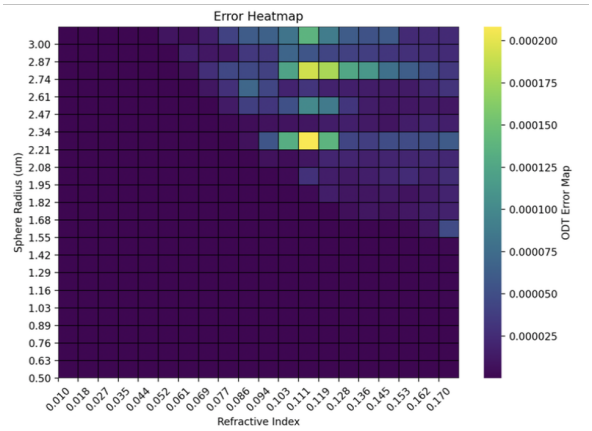

Fig. 12. ODT Error Heatmap

come harder to reconstruct the original image. For IDT, the error remains low under a certain radius; this behavior is also understandable and expected. Smaller radius means less perturbing because the light doesn't travel through the object's medium for too long. There is an interesting pattern that arises with IDT performing more accurately as refractive index increases, at least within this range of values. This observation was not expected. Some explanations for this are that intensity differences are less sensitive to absolute phase error, making it more robust in the face of greater phase perturbations caused by a higher refractive index change. This could imply that it is numerically more stable at higher RI contrast. Despite IDT lacking full field information, it could resolve boundaries and contrast transitions better because of the reconstruction algorithm. While, this could explain why IDT performs better than ODT at higher RI contrast, it is still unclear why IDT is performing better at higher RI constrast compared to itself at lower RI contrast.

3 FUTURE WORK

It is possible that there are mathematical errors in the code that reconstructs these images. The next step would just be going over the code with the literature and making sure the function is reconstructing exactly as it should be and there are no mathematical alterations that could be made to make these approximations more theoretically accurate. Beyond the scope of what this project though, these quantitative phase imaging techniques can be paired with other imaging techniques to resolve more information within an image. For example, it can be paired with Mid-Infrared Photothermal Microscopy. In Mid-infrared (MIR) photothermal microscopy, MIR light is used to excite molecular vibrations of specific polar bonds, generating regional heat changes, resulting in localized refractive index changes [4]. This gives rise to the ability to image for molecular specificity. This method can identify high concentrations of lipids or proteins in a cell. Unfortunately, this method of imaging only yields a low resolution 2D image. Hence, it is beneficial to pair this with diffraction tomography to get a 3D reconstruction of the internal cell components.

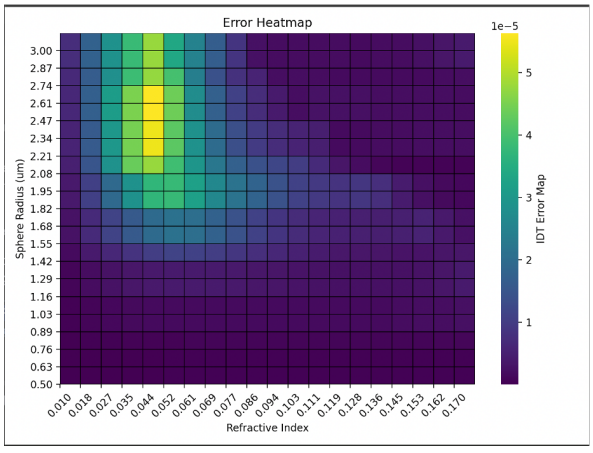

Fig. 13. IDT Error Heatmap

4 CONCLUSION

In this study, it was demonstrated that ODT and IDT work best under different parameters and which reconstruction method is best to used based on the sample type. When deciding which reconstruction algorithm is best given the initial parameters of one's sample, refer to Table 3.

Table 3. Conclusion

RI Constrast	Radius	Best Method
Small RI (< 0.09)	Small Radius ($< 1.5\ \mu m$)	Both
Large RI (> 0.09)	Small Radius ($< 1.5\ \mu m$)	Both
Large RI (> 0.09)	Large Radius ($> 1.5\ \mu m$)	IDT
Small RI (< 0.09)	Large Radius ($> 1.5\ \mu m$)	ODT

When the radius of the sphere is small enough, either approximate reconstruction algorithm would work because the perturbation is small enough anyways. For larger radius, the perturbation becomes more apparent and have greater affects, so the difference between a low RI contrast and a higher one becomes important. For reconstruction of an object with a lower RI contrast, ODT is better, and for an object with higher RI contrast, IDT is more useful.

5 ACKNOWLEDGMENTS

I would like to thank Professors Takuro Ideguchi for selecting me for this opportunity to intern in his laboratory this summer. I'd like to give a special thanks to Masato Fukushima for his patient guidance throughout my learning. I would also like to thank all of the members of the Ideguchi Group for their welcoming attitudes, as well as the staff members of UTRIP, and Friends of UTokyo, Inc. for their generous support.

6 REFERENCES

[1] K. Kim, et al., "Optical Diffraction Tomography Techniques for the Study of Cell Pathophysiology", *Journal for Biomedical Photonics and Engineering 2, 2.*2016.doi: 10.18287/JBPE16.02.020201

[2] P. Muller, M. Schurmann, J. Guck, "The Theory of Diffraction Tomography", *arXiv preprint https://doi.org/10.48550/arXiv.1507.00466,* 2016.

[3] R. Ling, et al., "High-throughput Intensity Diffraction Tomography with a Computational Microscope", *Biomedical Optics Express, 9, 5.* 2018. https://doi.org/10.1364/BOE.9.002130

[4] M. Tamamitsu "Mid-infrared Photothermal Quantitative Phase Imaging", *Doctoral Dissertation,* 2020.